Nucleation Dynamics of Phase-Change Memory Materials: Atomic Motion and Property Evolution

Nian-Ke Chen, Yu-Ting Liu, Xue-Peng Wang, and Xian-Bin Li*

Reversible phase transitions between crystalline and amorphous phases of phase-change memory (PCM) materials are the physical basis of PCM. Applications of PCM in multilevel memory, in-memory computing, and neuromorphic computing require a precise control of material's structure/property to achieve signals beyond binary (0/1), where recrystallization is the key process because it is smooth compared with violent amorphization. By molecular dynamic simulations and electronic structure analyses based on density functional theory, nucleation dynamics during recrystallization are investigated from the point of view of atomic motions and property evolutions. Atomic motions are examined individually rather than statistically. According to the results, an atomic picture of the growth of the nucleus is described in detail, where the competition between the potential seeds of nucleus plays a critical role. The electron polarization during recrystallization is mapped to the linearly aligned atom chains. Further analyses of the Born effective charge confirm the delocalization of the electrons in the atom chains. Also, a large p-orbital-axial Born effective charge is observed in long-range atom chains, which suggests a kind of resonance enhancement of electronic delocalization. These dynamics of nucleation in recrystallization provide references for the fine control of PCM performances.

Phase-change memory (PCM) continuously attracts attention due to its success in high-density storage class memory and new applications, such as in-memory computing and neuromorphic computing.[1–8] The basic principle of this technology is the reversible phase change between crystalline and amorphous phases accompanied with electronic or optical signal switching.[9] The stimuli to trigger the phase change can be electrical pulse, optical pulse, and external pressure.[9–16] The applications of PCM in commercialized high-density electronic memory and new-type neuromorphic computing demand finer controllability of the phase change.[8,17–19] In particular, recrystallization (SET operation) is not only the rate-limiting process of memory but also the key process to realize in-memory and neuromorphic computing.

Dr. N.-K. Chen, Y.-T. Liu, Dr. X.-P. Wang, Prof. X.-B. Li
State Key Laboratory of Integrated Optoelectronics
College of Electronic Science and Engineering
Jilin University
Changchun 130012, China
E-mail: lixianbin@jlu.edu.cn

The ORCID identification number(s) for the author(s) of this article can be found under https://doi.org/10.1002/pssr.202000441.

The most frequently used material in PCM devices is $Ge_2Sb_2Te_5$ (GST) alloy, which is regarded as the prototypical PCM material.[20,21] Except for the newly invented interface PCM based on the $[GeTe]_m–[Sb_2Te_3]_n–$ superlattice,[19,22–24] the crystalline phase utilized in conventional PCM devices is the metastable rock-salt phase whereas the most stable phase of GST is trigonal.[25] Recently, an intermedium vacancy-ordered phase is also discovered.[26–29] The mechanism of the recrystallization of GST has been widely investigated by both experiments and theoretical simulations. Especially, first-principles calculations and ab initio molecular dynamic (AIMD) simulations can provide insights into atomic-scale dynamics and thus have been frequently used.

It is revealed that most Ge and Sb atoms in amorphous GST form defective octahedrons or pyramids except one-third Ge atoms with tetrahedral configurations.[30–32] Atomic and electronic structures analyses suggest that both crystalline and amorphous phases are p-bonding dominant with octahedral configurations and fourfold rings.[33,34] The similarity of the two phases obviously would facilitate reversible phase changes. AIMD simulations reveal the early stage of nucleation, where fourfold rings are first formed and then connected to form ordered planar structures and finally turn into cubes.[35] The formation of planar structures is proposed to lower the interfacial energy between crystalline and amorphous clusters. GST is a nucleation-dominated material, but crystal growth becomes more important in nanoscale devices.[36,37] The AIMD simulations of the growth process suggest that the growth speed at the temperature of about 700 K is the fastest.[38–41] The simulated speed of growth is at the order of $m \cdot s^{-1}$ which is consistent with experiments.[37,42] As the simulations are performed with finite-size cells, percolation plays important roles in growth.[38] Up to now, the longest time of simulation reached 8.2 nanoseconds (ns) with 460 atoms in the cell.[39] Generally, these simulations indicate that the nucleation in GST is stochastic. Surprisingly, if a crystalline seed had previously existed in the simulation, then the recrystallization may be facilitated.[38] As for the distribution of vacancies during recrystallization, some reports found it is randomly distributed while some reports suggest that it is accumulated at the interfaces.[35,38,41,43,44] AIMD simulations also suggest that the recrystallization of GST can be optimized by the modulation of stimuli pulse and external pressure.[12,45–47] In brief, the

mechanism of recrystallization has been a long-term problem. Despite the numerous simulations and detailed analyses of recrystallization or nucleation, the dynamic picture at the atomic scale is still valuable to be studied from different points of view to clarify previous mechanisms or inspire new ideas to better control PCM devices.

In this Letter, we study the atomic motions and property evolutions of PCM material GST during the nucleation process by first-principles calculations and AIMD. The atomic motions are investigated at the scale of individual atoms by examining all the atoms one by one. Three types of behaviors of these atoms are classified and used to interpret the nucleation dynamics. The atomic motions suggest that the competition between the potential seeds of nucleus plays important roles in the nucleation of recrystallization. The evolutions of the properties are mapped to the evolution of atomic motifs, namely, the linearly aligned atom chains (LAACs). The relationship between the atomic motif and electronic property can be explained by Born effective charge (BEC). These pictures provide more detailed dynamics of nucleation at the atomic scale which may be used to control the PCM property with a finer precision.

Figure 1 shows the evolution of the energy, fourfold rings, normal bonds, and wrong bonds during the MD simulation of recrystallization from a melt-quenched amorphous phase. As the model used in this work contains 194 atoms, recrystallization in such a finite-size cell is dominated by nucleation rather than the growth process. Therefore, the expression of "nucleation" is used instead in the following sections. The finite-size effects may influence the speed of growth, the degree of crystallization, and the formation of multiple nuclei.[48] However, the reported dynamics of the nucleation process in different models are very similar and thus the study of nucleation dynamics in this work is still reliable.[33,38–41,43] The energy and wrong bonds decrease and the fourfold rings and normal bonds increase during nucleation. According to these characterizations, the nucleation begins at about 40 ps and is nearly completed at about 180 ps. The point of time for nucleation is different from previous ones because the nucleation is stochastic.[33,35,38,39] The distribution of the vacancies or voids is partially accumulated in our simulation (see Figure S1, Supporting Information). As the evolutions of the structural characteristics, such as the energy, the bonds, the bond angles, the pair correlation functions, and the rings, are consistent with previous reports,[35,39,40] we do not repeat their discussions any more.

Previous studies of structural evolution mainly focus on the statistical analyses of a large number of atoms where behaviors of an individual atom are omitted by the average effect. Here, we track the motions of individual atoms in the simulation cell one by one to see what happens to an atom during the nucleation process. Considering that an atom nearly stops moving when it forms a stable nucleus, we take its position at the final time (300 ps) as a reference point. Then, we trace back its position to the initial time by calculating the distance between the reference position and the position at time t, which is called the trace-back-distance here. **Figure 2** shows several representative examples of the results. It suggests that the motions of atoms can be classified into three types during nucleation.
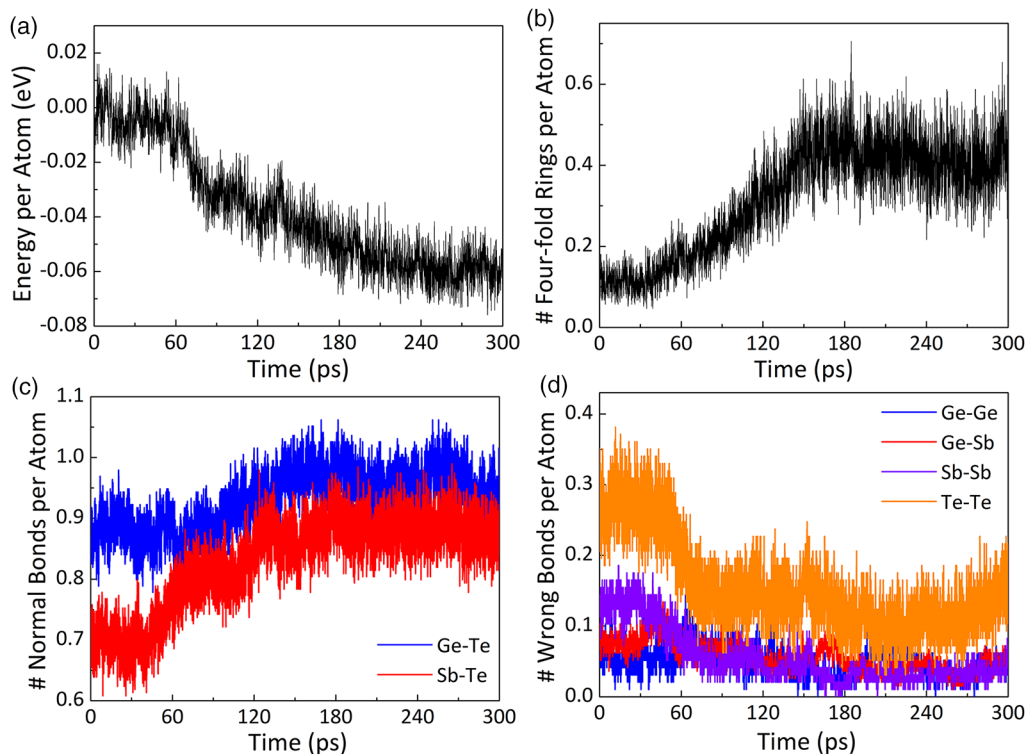

Figure 1. a-d) Time evolution of energy (a), number of fourfold rings (b), normal bonds (c), and wrong bonds (d) of $Ge_2Sb_2Te_5$ during the MD of nucleation in recrystallization.

ADVANCED
SCIENCE NEWS
www.advancedsciencenews.com
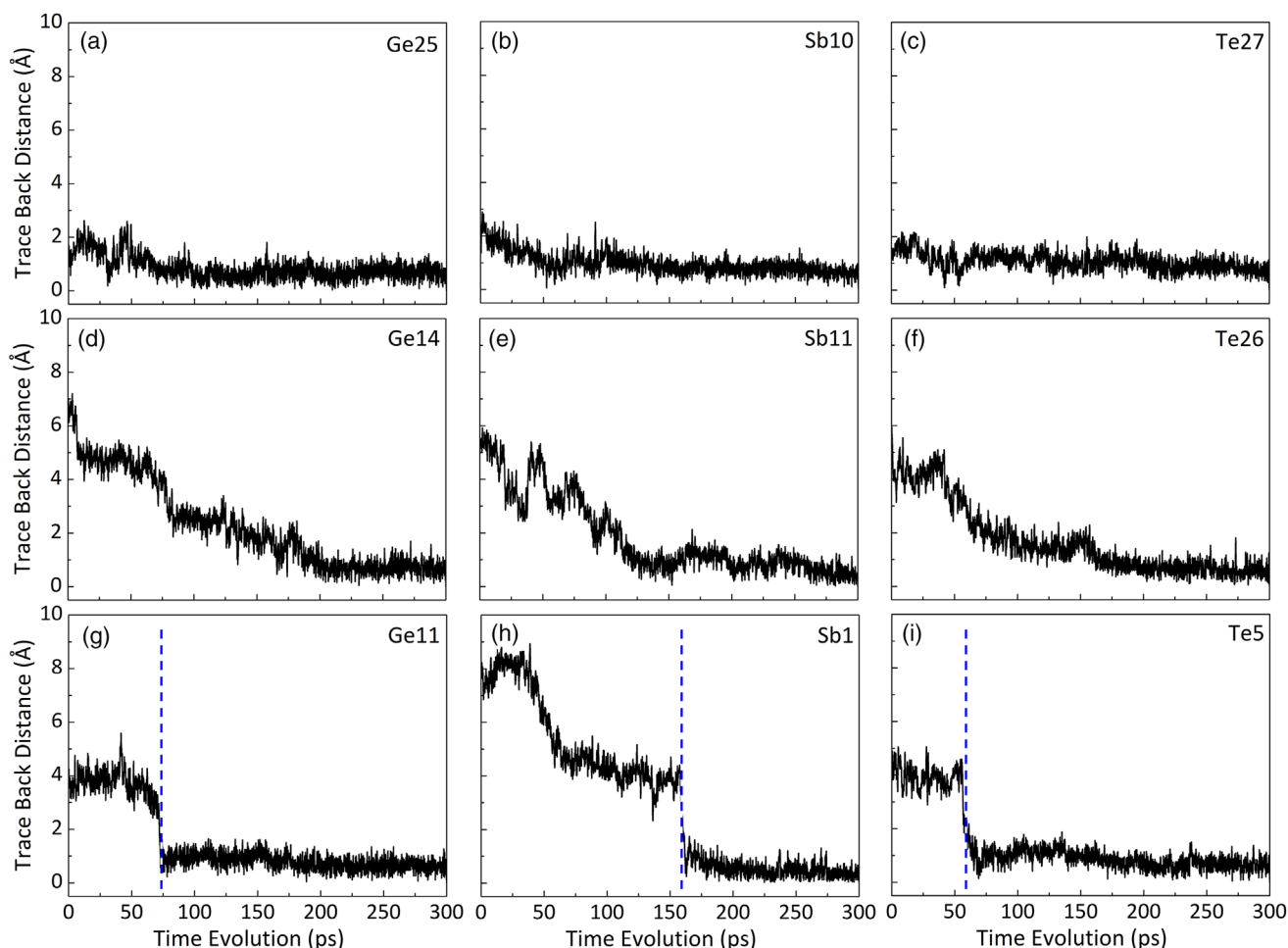
pss rrl
physica status solidi

www.pss-rapid.com

Figure 2. Representative examples of trace-back-distance analyses during nucleation. The blue dashed line indicates the abrupt movement from one metastable position to another.

For the first type (see Figure 2a–c), atoms stay in their initial positions because nucleation takes place from them. In fact, they are part of the fourfold rings in the amorphous phase that is formed during the melt-quenching process. Previous reports also identified fourfold rings and cubes as the facilitators of fast nucleation.[33,35] Therefore, the stable motifs, such as the fourfold rings and cubes, can be regarded as the potential seeds for nucleation. In fact, there are many randomly distributed fourfold rings in the amorphous phase. But most of them could move, for example, rotate, dissipate, and reconstruct, to finally form an ordered nucleus. Therefore, only one specific seed can be identified from the pictures in this calculation. As such, the proportion of atoms in this pre-existing seed is only about 3%.

For the second type (see Figure 2d–f), atoms move gradually to their destinations (i.e., the nucleus). These atoms indicate the growth of the nucleus where atoms migrate from amorphous regions to the nucleus. The smooth motions may correspond to the atomic diffusion in the supercooled liquid or the rotation of fourfold rings. We can call them analog behavior. Most of the atoms (about 73%) move in such a way.

For the third type (see Figure 2g–i), it is unexpected that atoms move abruptly rather than gradually from relatively stable

positions to the nucleus. The front platform of the trace-back-distance means that the atoms are trapped in relatively stable positions. We checked the motions of these atoms by hand and found that most of them moved from a ring (or cube) to another ring (or cube). As mentioned earlier, these relatively stable motifs can act as potential seeds for nucleation. As such, the third-type motions suggest a competition between the potential seeds. As is known, GST is nucleation dominated. The orientations of different potential seeds (octahedrons, rings, or cubes) often conflict with each other. Then, the competition should be inevitable. One seed decomposes and then reconstructs into another new seed and thus leads to the growth of the nucleus. Compared with the second-type motion, the third one may need a larger activation energy to overcome the trapping effect. The proportion of the third-type atoms is about 24%, suggesting they should also play significant roles.

Generally, once an atom participates in forming a stable nucleus, it is equivalent to be trapped in an energy-minimum position and would temporarily stop diffusion. Similarly, during the MD simulation of nucleation, when some atoms stop diffusion, they can approximately be regarded as part of the nucleus. **Figure 3** shows that the atoms reach their stable positions.
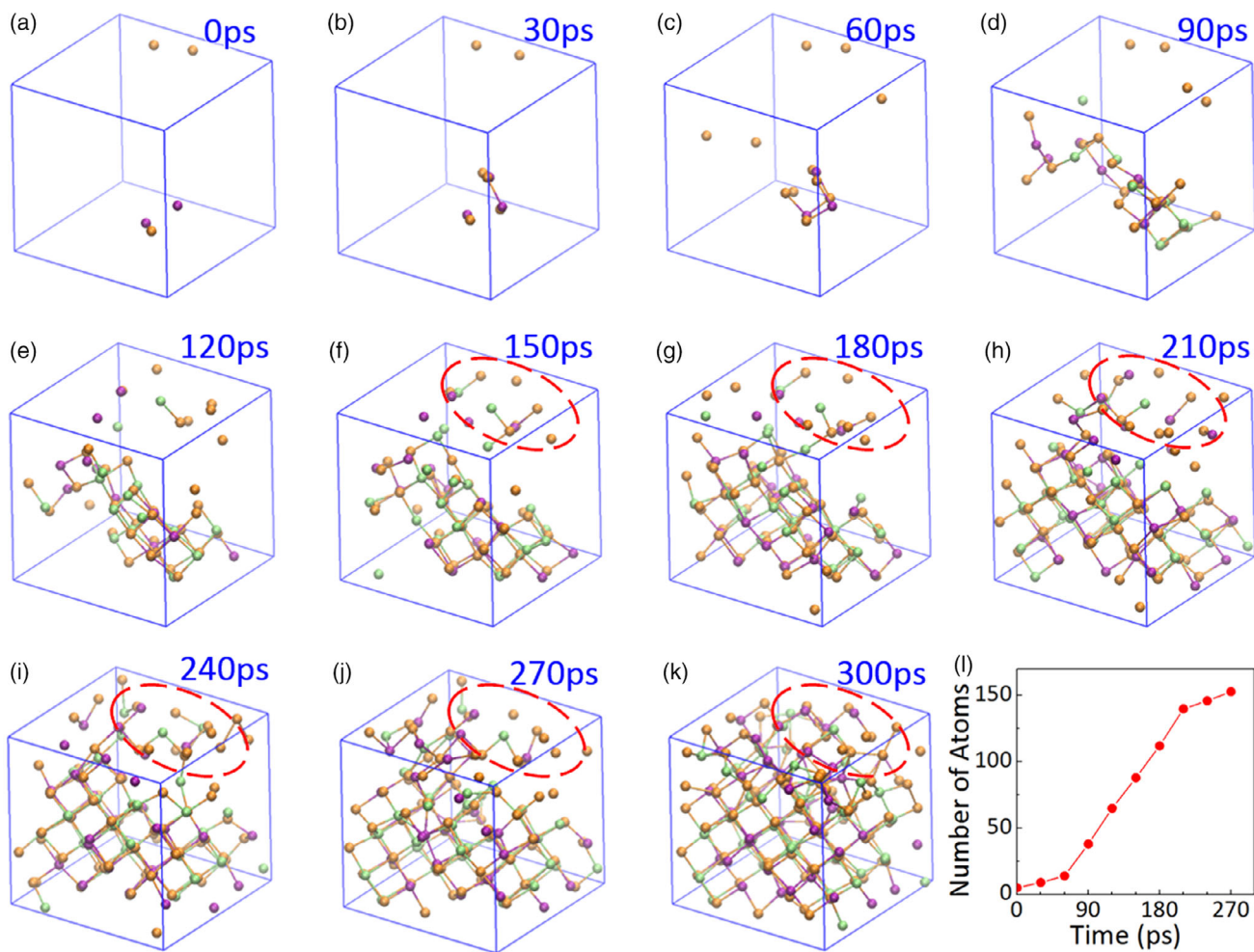
Figure 3. a–k) Snapshots of the nucleus in MD. Green, purple, and orange balls represent Ge, Sb, and Te atoms, respectively. l) The number of atoms in nucleus.

Obviously, these atoms can indeed indicate the nucleation process. Figure 3l shows the number of atoms that participated in the nucleation. The growth of the nucleus mainly takes place from 60 to 210 ps. Then the nucleus still continuously grows. According to Figure 1, the number of normal bonds and wrong bonds does not change after 180 ps. A possible explanation is that the nucleation process after 180 ps is dominated by the rotation of some motifs. In addition, there is another small nucleus in the cell (see the dashed circles in Figure 3). Finally, the two nuclei conflict with each other and thus hinder complete nucleation. As it is very hard for such a big nucleus to rotate, the smaller nucleus may also dissipate and reconstruct into the bigger one, which of course will take a very long time. The conflict of nuclei with different orientations has been observed previously in a simulation using 460 atoms, where the growth of a nuclei was blocked for 1 ns.[38]

The property of PCM materials gradually changes with nucleation, which enables the applications in multilevel memory, in-memory computing, and neuromorphic computing. In these applications, the multilevel signal is controlled by the volume of recrystallized phases. However, the properties of PCM materials

also change with variations of local configurations, which may influence the controllability and reliability of PCM devices. Therefore, the relationship between local structures and electronic/optical properties during nucleation has always been a concern.

Here, we study the evolution of electronic polarization. **Figure 4**a shows the calculated relative reflectivity of the structures selected from the MD trajectory. The structures are relaxed to their locally equilibrium positions before calculating the property. Then the values at 800 nm are adopted to draw the time evolution behavior, as shown in Figure 4b. When comparing the time evolutions of the reflectivity and the energy, we find the mismatch between them. The energy obviously decreases before 90 ps, implying the change of local atomic structures. But the reflectivity nearly remains unchanged. It may be understood as the incubation process for nucleation. For this process, the changes of structure and property may mismatch. Although reflectivity is unchanged, the decreased energy clearly indicates the reordering of local structures, such as the breaking (forming) of wrong (normal) bonds. For example, it has been reported that by applying a very low incubation voltage before the SET operation, the crystallization speed can be reduced to 500 ps.[47]
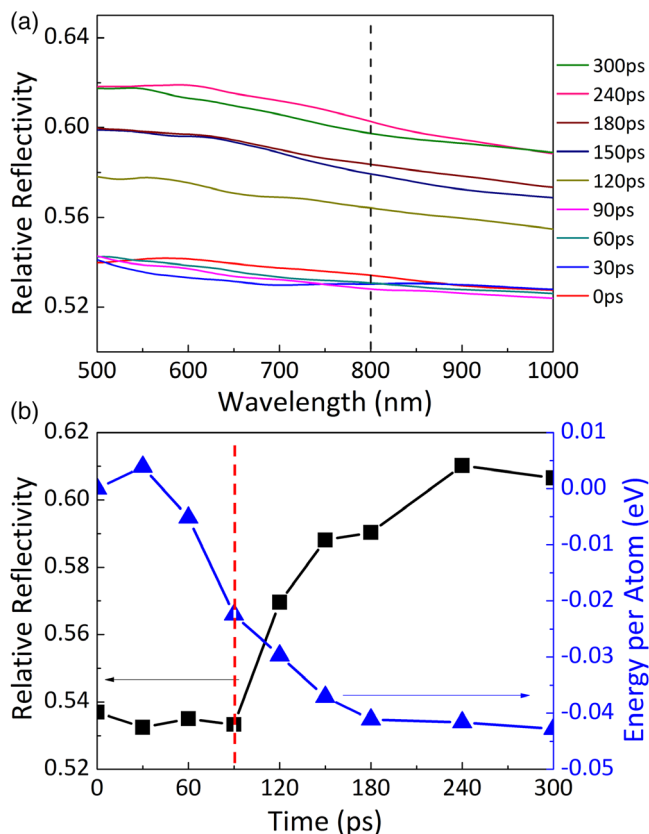
Figure 4. a) The change of the relative reflectivity of GST during the nucleation. b) Time evolution of the change of the relative reflectivity at 800 nm (black squares) and energy (blue triangles).

Figure 5. a) The number of LAACs during nucleation. The 2D plot can be found in Figure S2, Supporting Information. b) Time evolutions of the reflectivity (black squares) and the number of aligned bonds (green dots) during nucleation. The number of the aligned bonds is calculated from the LAACs. For example, an *n*-atom chain contains (*n* − 1)-aligned bonds.

In previous studies, we have shown the strong electronic polarization of the LAACs in amorphous GST.[49] The LAAC is formed by linearly connected atoms, where the bonding *p*-orbitals are aligned along the axial direction. Even in the amorphous phase of GST, there exist a lot of short LAACs. Electronic structure analyses suggest that electron polarization in these LAACs is relatively strong. Therefore, we analyze the time evolution and the distribution of LAACs during nucleation (see **Figure 5**a). The large amount of three-atom chains in the amorphous phase is contributed by the octahedral or defective octahedral motifs. Then, longer LAACs gradually increase with nucleation. The odd-number LAACs are predominant because vacancies often are formed near Te atoms. The number of three-atom chains is always considerable due to the presence of distortions and vacancies. The linearly aligned *p*-orbitals have been demonstrated to enhance optical matrix elements.[50] If suppose the bonding in the LAACs is the origin of strong electron polarization, the number of linearly aligned bonds in LAACs can approximately represent reflectivity. Figure 5b shows the reflectivity with the number of aligned bonds during nucleation. The time evolutions of them are consistent.

The BEC can evaluate electronic polarization along a specific direction at the atomic scale, whereas reflectivity is an average quantity. In the crystalline GST, an atom participates in three different LAACs along three orthogonal directions. To fairly
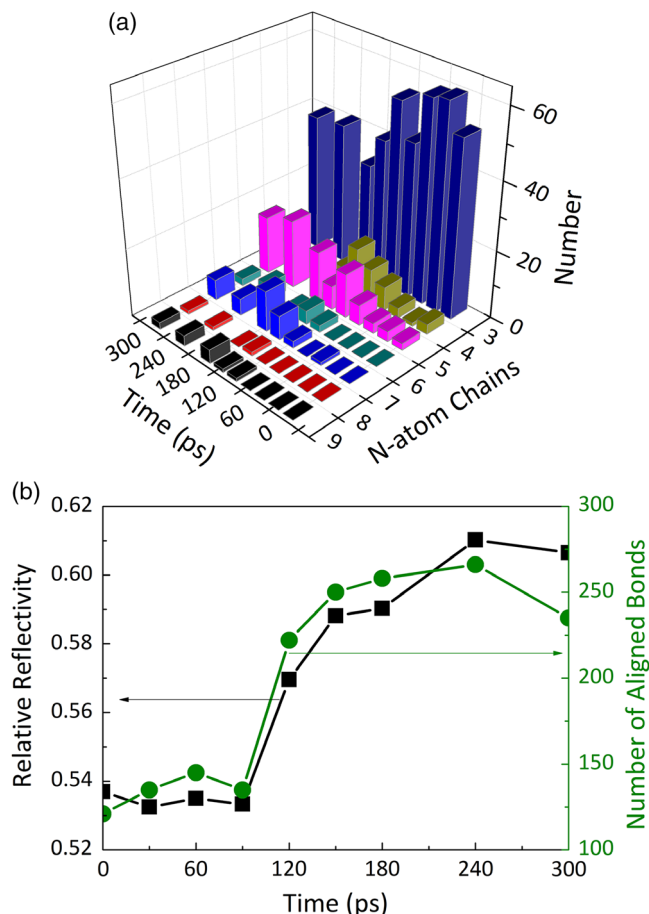
evaluate the relationship between BEC and linearly aligned *p*-orbitals, the BEC in the LAAC should be the component that is projected to the axial direction of the chain (called the *p*-orbital-axial BEC here). **Figure 6**a shows the *p*-orbital-axial BEC of LAACs in crystalline phases and the average BEC of the atoms in the amorphous phase. Due to the existence of vacancies, there are also many short LAACs, i.e., the three-atom chains and five-atom chains. Although these LAACs are short, the *p*-orbital-axial BEC of them is still larger than the average BEC in the amorphous phase. For the long LAACs (percolated in the periodic supercell), the *p*-orbital-axial BEC is obviously further enhanced, suggesting that the strong electron polarization is also related to the length of LAACs. Therefore, the less the vacancies, the higher the electron polarization in crystalline GST, which is consistent with experiments.[51] Figure 6b shows the time evolutions of reflectivity and BEC during nucleation. The agreement of reflectivity and BEC during nucleation is consistent with the previous theory.[52] Therefore, LAACs may govern the optical property.

Several mechanisms have been previously proposed to explain the optical property of PCM materials, such as the resonant bonding,[53] metavalent bonding,[54] hyperbonding,[55] and
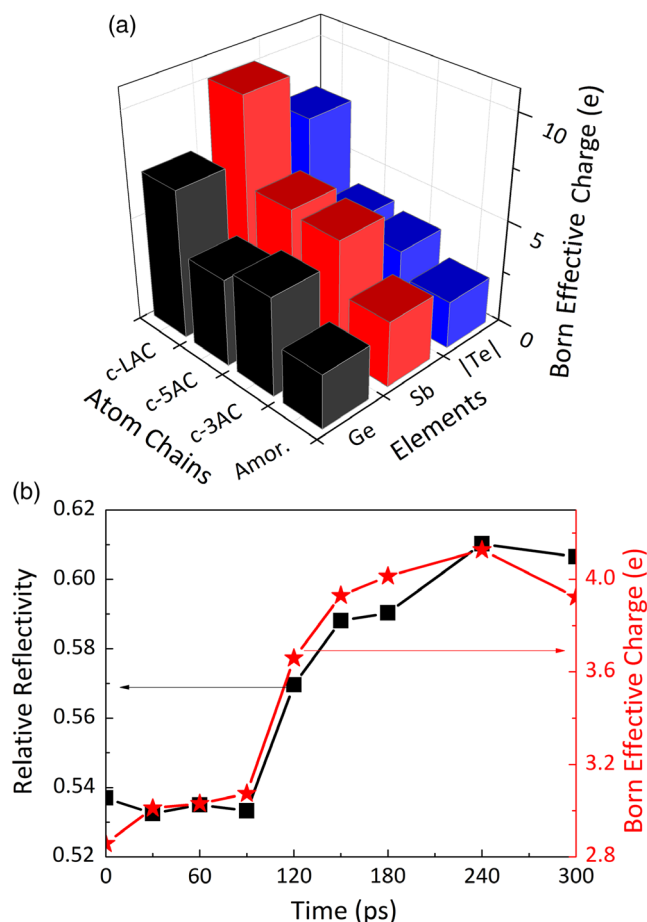
ADVANCED
SCIENCE NEWS
www.advancedsciencenews.com

physica
pss status solidi rrl
www.pss-rapid.com

Figure 6. a) The average BEC of the atoms in amorphous (Amor.) and crystalline (c-) phases. For the amorphous phase, the average of the trace of BEC tensor is adopted. The crystalline phase is the rock-salt model before MD simulations. One atom would participate in three different LAACs along different directions. To evaluate the relationship between BEC and aligned *p*-orbitals, the BEC in the crystalline phase is projected to the axial direction of LAACs, namely the *p*-orbital-axial BEC (see main text). c-3AC, c-5AC, and c-LAC present three-atom chains, five-atom chains, and long-atom chains in the crystalline phase. We note that the seven-atom chains in our periodic model is percolated and thus represent infinitely long atom chains (c-LAC). The 2D plot is found in Figure S3, Supporting Information. b) Time evolutions of the relative reflectivity (black squares) and the root of the mean square of BEC (red stars) during nucleation.

three-center–four-electron bonding.[56] In contrast, some reports regard bonding as a competing ionic and covalent bonding,[57] whereas some reports believe that the optical property can be explained by the Penn gap rule.[58] Recently, Jones explained the property of GST by the orbital property of valence electrons and a near-free electron model without invoking different bonding mechanisms.[59] Compared with the atoms not forming LAACs, the relatively larger *p*-orbital-axial BEC in short LAACs suggests that electrons are delocalized in the short aligned *p*-orbitals. The resonant bonding is proposed based on the half-filled *p*-orbitals, where the electrons can move between adjacent bonds. The metavalent bonding is proposed from the point

of view of electrons transferred and shared between atoms,[60] where the metavalent bonding seems to be the intermediate between the metallic and covalent or ionic bonding. The multi-center three-center–four-electron hyperbonding is formed by the lone-pair electrons and antibonding orbitals. Both the metavalent (or resonant) bonding and hyperbonding suggest the delocalization of bonding electrons and thus this may be used to explain this phenomenon. In particular, compared with the *p*-orbital-axial BEC in the short LAACs, the *p*-orbital-axial BEC in the long (percolated) LAACs is dramatically enhanced by nearly 100%, see Figure 6a. Such an amplification behavior indeed suggests a feature of "resonance enhancement" of electronic delocalization, at least in the long LAACs.

As mentioned earlier, both the fast crystallization and the subsequently large optical property change originate from *p*-bonding. If doped/alloyed with elements that disturb *p*-bonding, such as C, Si, and Cu, the amorphous phase of PCM materials becomes more stable.[61–64] In contrast, if doped with elements whose bonding is similar with *p*-bonding, such as Ti and Sc, the speed of crystallization is further enhanced due to the formation of the robust seeds of nucleus (i.e., the octahedral motifs).[18,65–67]

In conclusion, first-principles calculations and AIMD are used to investigate the atomic motion and property evolution during nucleation in the recrystallization of GST. The motions of individual atoms are classified into three types and mapped to the dynamics of nucleation: the diffusion-less seeds for nucleation, the gradual movement for the growth of the nucleus, and the abrupt movement for competition between metastable motifs. Compared with second-type motions, third-type motions should overcome larger energy barriers and thus should be a key factor of fast nucleation. Analyses and comparisons of LAACs, the relative reflectivity, and the BEC demonstrate that the increase in LAACs is responsible for the increase in reflectivity during nucleation. The result also is evidence that the linearly aligned *p*-orbitals enable the delocalization of electrons. Especially, the large *p*-orbital-axial BEC in long-range LAACs suggests a kind of resonance enhancement of electronic delocalization. These results provide further detailed dynamics, including atomic movements and the evolution of basic motifs and electronic properties, during the nucleation of PCM GST.

Experimental Section

Density functional theory (DFT) calculations were carried out using the Vienna Ab-initio Simulation Package (VASP).[68,69] Projector-augmented-wave (PAW) pseudopotentials and generalized-gradient-approximation (GGA) exchange-correlation functional developed by Perdew, Burke, and Ernzerhof (PBE) were adopted.[70,71] The cut-off energy for plane-wave expansion was 240 eV. The Monkhorst–Pack grid of *k*-points of $1 \times 1 \times 1$ and $2 \times 2 \times 2$ were used for molecular dynamics and property calculations, respectively. More details on simulations and analyses are found in Supporting Information.

Supporting Information

Supporting Information is available from the Wiley Online Library or from the author.

Conflict of Interest

The authors declare no conflict of interest.

[1] J. Feldmann, N. Youngblood, C. D. Wright, H. Bhaskaran, W. H. P. Pernice, *Nature* **2019**, *569*, 208.

[2] P. Noé, C. Vallée, F. Hippert, F. Fillot, J.-Y. Raty, *Semicond. Sci. Technol.* **2018**, *33*, 013002.

[3] A. Sebastian, T. Tuma, N. Papandreou, M. Le Gallo, L. Kull, T. Parnell, E. Eleftheriou, *Nat. Commun.* **2017**, *8*, 1115.

[4] T. Tuma, A. Pantazi, M. Le Gallo, A. Sebastian, E. Eleftheriou, *Nat. Nanotechnol.* **2016**, *11*, 693.

[5] C. D. Wright, Y. Liu, K. I. Kohary, M. M. Aziz, R. J. Hicken, *Adv. Mater.* **2011**, *23*, 3408.

[6] X. Yin, T. Steinle, L. Huang, T. Taubner, M. Wuttig, T. Zentgraf, H. Giessen, *Light: Sci. Appl.* **2017**, *6*, e17016.

[7] Q. Zhang, H. Yu, M. Barbiero, B. Wang, M. Gu, *Light: Sci. Appl.* **2019**, *8*, 42.

[8] W. Zhang, R. Mazzarello, M. Wuttig, E. Ma, *Nat. Rev. Mater.* **2019**, *4*, 150.

[9] M. Wuttig, N. Yamada, *Nat. Mater.* **2007**, *6*, 824.

[10] S. Caravati, M. Bernasconi, T. Kühne, M. Krack, M. Parrinello, *Phys. Rev. Lett.* **2009**, *102*, 205502.

[11] A. Kolobov, J. Haines, A. Pradel, M. Ribes, P. Fons, J. Tominaga, Y. Katayama, T. Hammouda, T. Uruga, *Phys. Rev. Lett.* **2006**, *97*, 035701.

[12] Z. Sun, J. Zhou, A. Blomqvist, B. Johansson, R. Ahuja, *Phys. Rev. Lett.* **2009**, *102*, 075504.

[13] Z. Sun, J. Zhou, Y. Pan, Z. Song, H. K. Mao, R. Ahuja, *Proc. Natl. Acad. Sci. USA* **2011**, *108*, 10410.

[14] M. Wuttig, *Nat. Mater.* **2005**, *4*, 265.

[15] M. Xu, Y. Q. Cheng, L. Wang, H. W. Sheng, Y. Meng, W. G. Yang, X. D. Han, E. Ma, *Proc. Natl. Acad. Sci. USA* **2012**, *109*, E1055.

[16] J. H. Zhao, X. B. Li, Q. D. Chen, Z. G. Chen, H. B. Sun, *Mater. Today Nano* **2020**, *11*, 100078.

[17] N.-K. Chen, X.-B. Li, *Chin. Phys. B* **2019**, *28*, 104202.

[18] K. Ding, J. Wang, Y. Zhou, H. Tian, L. Lu, R. Mazzarello, C. Jia, W. Zhang, F. Rao, E. Ma, *Science* **2019**, *366*, 210.

[19] X. B. Li, N. K. Chen, X. P. Wang, H. B. Sun, *Adv. Funct. Mater.* **2018**, *28*, 1803380.

[20] N. Yamada, *Phys. Status Solidi B* **2012**, *249*, 1837.

[21] N. Yamada, E. Ohno, K. Nishiuchi, N. Akahira, M. Takao, *J. Appl. Phys.* **1991**, *69*, 2849.

[22] T. C. Chong, L. P. Shi, R. Zhao, P. K. Tan, J. M. Li, H. K. Lee, X. S. Miao, A. Y. Du, C. H. Tung, *Appl. Phys. Lett.* **2006**, *88*, 122114.

[23] J. Momand, R. Wang, J. E. Boschker, M. A. Verheijen, R. Calarco, B. J. Kooi, *Nanoscale* **2017**, *9*, 8774.

[24] R. E. Simpson, P. Fons, A. V. Kolobov, T. Fukaya, M. Krbal, T. Yagi, J. Tominaga, *Nat. Nanotechnol.* **2011**, *6*, 501.

[25] T. Matsunaga, N. Yamada, Y. Kubota, *Acta Crystallogr., Sect. B* **2004**, *60*, 685.

[26] V. Bragaglia, F. Arciprete, W. Zhang, A. M. Mio, E. Zallo, K. Perumal, A. Giussani, S. Cecchi, J. E. Boschker, H. Riechert, S. Privitera, E. Rimini, R. Mazzarello, R. Calarco, *Sci. Rep.* **2016**, *6*, 23843.

[27] U. Ross, A. Lotnyk, E. Thelander, B. Rauschenbach, *Appl. Phys. Lett.* **2014**, *104*, 121904.

[28] X.-P. Wang, X.-B. Li, N.-K. Chen, Q.-D. Chen, X.-D. Han, S. Zhang, H.-B. Sun, *Acta Mater.* **2017**, *136*, 242.

[29] B. Zhang, X. P. Wang, Z. J. Shen, X. B. Li, C. S. Wang, Y. J. Chen, J. X. Li, J. X. Zhang, Z. Zhang, S. B. Zhang, X. D. Han, *Sci. Rep.* **2016**, *6*, 25453.

[30] S. Caravati, M. Bernasconi, T. D. Kühne, M. Krack, M. Parrinello, *Appl. Phys. Lett.* **2007**, *91*, 171906.

[31] A. V. Kolobov, P. Fons, A. I. Frenkel, A. L. Ankudinov, J. Tominaga, T. Uruga, *Nat. Mater.* **2004**, *3*, 703.

[32] M. Krbal, A. V. Kolobov, P. Fons, J. Tominaga, S. R. Elliott, J. Hegedus, T. Uruga, *Phys. Rev. B* **2011**, *83*, 054203.

[33] J. Hegedus, S. R. Elliott, *Nat. Mater.* **2008**, *7*, 399.

[34] M. Xu, Y. Q. Cheng, H. W. Sheng, E. Ma, *Phys. Rev. Lett.* **2009**, *103*, 195502.

[35] T. H. Lee, S. R. Elliott, *Phys. Rev. Lett.* **2011**, *107*, 145702.

[36] M. Salinga, E. Carria, A. Kaldenbach, M. Bornhofft, J. Benke, J. Mayer, M. Wuttig, *Nat. Commun.* **2013**, *4*, 2371.

[37] A. Sebastian, M. Le Gallo, D. Krebs, *Nat. Commun.* **2014**, *5*, 4314.

[38] J. Kalikka, J. Akola, R. O. Jones, *Phys. Rev. B* **2014**, *90*, 184109.

[39] J. Kalikka, J. Akola, R. O. Jones, *Phys. Rev. B* **2016**, *94*, 134105.

[40] J. Kalikka, J. Akola, J. Larrucea, R. O. Jones, *Phys. Rev. B* **2012**, *86*, 144113.

[41] I. Ronneberger, W. Zhang, H. Eshet, R. Mazzarello, *Adv. Funct. Mater.* **2015**, *25*, 6407.

[42] J. Orava, A. L. Greer, B. Gholipour, D. W. Hewak, C. E. Smith, *Nat. Mater.* **2012**, *11*, 279.

[43] T. H. Lee, S. R. Elliott, *Phys. Rev. B* **2011**, *84*, 094124.

[44] W. Zhang, A. Thiess, P. Zalden, R. Zeller, P. H. Dederichs, J. Y. Raty, M. Wuttig, S. Blugel, R. Mazzarello, *Nat. Mater.* **2012**, *11*, 952.

[45] P. S. Branicio, K. Bai, H. Ramanarayan, D. T. Wu, M. B. Sullivan, D. J. Srolovitz, *Phys. Rev. Mater.* **2018**, *2*, 043401.

[46] G. Eising, A. Pauza, B. J. Kooi, *Cryst. Growth Des.* **2012**, *13*, 220.

[47] D. Loke, T. H. Lee, W. J. Wang, L. P. Shi, R. Zhao, Y. C. Yeo, T. C. Chong, S. R. Elliott, *Science* **2012**, *336*, 1566.

[48] I. Ronneberger, W. Zhang, R. Mazzarello, *MRS Commun.* **2018**, *8*, 1018.

[49] N.-K. Chen, X.-B. Li, X.-P. Wang, W. Q. Tian, S. Zhang, H.-B. Sun, *Acta Mater.* **2018**, *143*, 102.

[50] B. Huang, J. Robertson, *Phys. Rev. B* **2010**, *81*, 081204R.

[51] M. Wuttig, D. Lusebrink, D. Wamwangi, W. Welnic, M. Gillessen, R. Dronskowski, *Nat. Mater.* **2007**, *6*, 122.

[52] G. Lucovsky, R. M. White, *Phys. Rev. B* **1973**, *8*, 660.

[53] K. Shportko, S. Kremers, M. Woda, D. Lencer, J. Robertson, M. Wuttig, *Nat. Mater.* **2008**, *7*, 653.

[54] M. Zhu, O. Cojocaru-Mirédin, A. M. Mio, J. Keutgen, M. Küpers, Y. Yu, J.-Y. Cho, R. Dronskowski, M. Wuttig, *Adv. Mater.* **2018**, *30*, 1706735.

[55] T. H. Lee, S. R. Elliott, *Adv. Mater.* **2020**, *32*, 2000340.

[56] A. V. Kolobov, P. Fons, J. Tominaga, S. R. Ovshinsky, *Phys. Rev. B* **2013**, *87*, 165206.

[57] S. Mukhopadhyay, J. Sun, A. Subedi, T. Siegrist, D. J. Singh, *Sci. Rep.* **2016**, *6*, 25981.

[58] K. Shimakawa, L. Střižik, T. Wagner, M. Frumar, *APL Mater.* **2015**, *3*, 041801.

[59] R. O. Jones, *Phys. Rev. B* **2020**, *101*, 024103.

[60] J. Y. Raty, M. Schumacher, P. Golub, V. L. Deringer, C. Gatti, M. Wuttig, *Adv. Mater.* **2019**, *31*, e1806280.

[61] N.-K. Chen, X.-B. Li, X.-P. Wang, M.-J. Xia, S.-Y. Xie, H.-Y. Wang, Z. Song, S. Zhang, H.-B. Sun, *Acta Mater.* **2015**, *90*, 88.

[62] Q. Hubert, C. Jahan, A. Toffoli, G. Navarro, S. Chandrashekar, P. Noé, D. Blachier, V. Sousa, L. Perniola, J. F. Nodin, A. Persico, R. Kies, S. Maitrejean, A. Roule, E. Henaff, M. Tessaire, P. Zuliani, R. Annunziata, G. Pananakakis, G. Reimbold, B. De Salvo, in *IEEE Int. Memory Workshop*, Milan, Italy **2012**, p. 1.

[63] Y. Sutou, T. Kamada, M. Sumiya, Y. Saito, J. Koike, *Acta Mater.* **2012**, *60*, 872.

[64] X. P. Wang, N. K. Chen, X. B. Li, Y. Cheng, X. Q. Liu, M. J. Xia, Z. T. Song, X. D. Han, S. B. Zhang, H. B. Sun, *Phys. Chem. Chem. Phys.* **2014**, *16*, 10810.

[65] F. Rao, K. Ding, Y. Zhou, Y. Zheng, M. Xia, S. Lv, Z. Song, S. Feng, I. Ronneberger, R. Mazzarello, W. Zhang, E. Ma, *Science* **2017**, *358*, 1423.

[66] X.-P. Wang, X.-B. Li, N.-K. Chen, J. Bang, R. Nelson, C. Ertural, R. Dronskowski, H.-B. Sun, S. Zhang, *npj Comput. Mater.* **2020**, *6*, 31.

[67] M. Zhu, M. Xia, F. Rao, X. Li, L. Wu, X. Ji, S. Lv, Z. Song, S. Feng, H. Sun, S. Zhang, *Nat. Commun.* **2014**, *5*, 4086.

[68] G. Kresse, J. Furthmuller, *Comput. Mater. Sci.* **1996**, *6*, 15.

[69] G. Kresse, D. Joubert, *Phys. Rev. B* **1999**, *59*, 1758.

[70] P. E. Blochl, *Phys. Rev. Condens. Matter* **1994**, *50*, 17953.

[71] J. P. Perdew, K. Burke, M. Ernzerhof, *Phys. Rev. Lett.* **1996**, *77*, 3865.